UCLA

PARTICLE-LADEN FLOWS

FINAL REPORT

Project Team
UCLA Applied Math REU
Kali Allison
Thomas Crawford
Saro Meguerdijian
Wylie Rosenthal
Gilberto Urdaneta

Project Advisors: Dr. Sungyon Lee, Dr. Aliki Mavromoustaki
Project Director: Dr. Andrea L. Bertozzi

August 2012

Abstract

We present an experimental study which investigates the motion of bi-disperse suspensions consisting of ceramic and glass beads in PDMS oil flowing down an inclined plane under the influence of gravity. We perform a parametric study in which we vary the inclination angle of the plane, the total particle volume fraction, and the relative ratio of glass to ceramic beads. Both types of beads used are denser than the oil. Mono-disperse suspensions of negatively buoyant particles give rise to three regimes: a 'settled' regime in which particles settle to the substrate, a 'ridged' regime in which particles settle to the front of the flow, and a transient, 'well-mixed' regime in which settling does not occur. A similar trend is observed in the current study in which lower inclination angles and higher concentrations of the ceramic beads favor the settled regime. Furthermore, the addition of a second particle species induces a striking effect in which the heavier ceramic beads migrate on top of the lighter glass beads; this phenomenon is thought to be the result of competing forces in the direction normal to the flow arising from gravitational settling and shear-induced migration. We also discuss the effect of experimental parameters on the location of the front versus time, as well as changes in the fingering instability.

Table of Contents

1 IMPACT

The flow of particle-laden films has applications in a variety of fields, ranging from geophysics to industrial mining to the pharmaceutical industry. Geophysically significant slurries, including lahars and other debris flows, occur commonly, and in industry particle separators are used to refine slurries into their constituent parts. Past work building a theoretical framework of the behavior of these slurries has focused on pure granular flows and pure viscous liquid flows. Relatively few have dealt with the gravity-driven flow of particle-laden films. In order to fully characterize the flow of a slurry down an incline, models must take into account the propagation of particles within a mixture, which often differs from the overall flow of the fluid due to migration effects. This leads to variation in the concentration of particles within the thin film and to deviations from the clear fluid model.

2 BACKGROUND

Herbert E. Huppert produced an accurate model for fluid flow velocity and front wavelength[1]. A fluid's position on the ramp is predicted to be directly proportional to $t^{\frac{1}{3}}$. This model relies on the lubrication theory[2] and the approximations underlying it. Huppert predicts that the position of the front, x, is less than $x_N = (9A^2 g \sin\alpha/4\nu)^{\frac{1}{3}} t^{\frac{1}{3}}$ (eqn. 9) derived below.

The momentum equation for a fluid moving down an incline plane is given by

$$0 = g\sin\alpha + \nu u_{zz} \tag{1}$$

when ignoring the surface tension and contact line effects. The momentum of the fluid is dependent on the incline angle α, the fluids dynamic viscosity coefficient ν, and shear acceleration u_{zz}. Using conservation laws for volume and momentum a nonlinear partial differential equation for the height of the fluid is written

$$0 = h_t + (g\sin(\alpha/\nu))h^2 h_x \tag{2}$$

or equivalently

$$h(x,t) = \left(-\frac{h_t}{H_x g}\csc(\alpha/\nu)\right)^{1/2} \tag{3}$$

This equation leads to a continuity equation calculating the cross sectional area A of the fluid

$$A = \int_0^{x_N(t)} H(x,t)dx \tag{4}$$

[1]Huppert, "Flow and instability of a viscous current down a slope", Nature 1982
[2]Batchelor, G. K. *An introduction to fluid Dynamics*,Cambridge University Press

The limits of integration go from the starting position x to the current position, $x_n(t)$, the position at a given time. By rearranging equation 2 the velocity of the fluid can be determined

$$\frac{dx}{dt} = (g\sin(\alpha/\nu))h^2 \tag{5}$$

Given an initial height, $h(x,0) = f(x)$, and initial position, x_0, the position of the flow is given as

$$x = x_0 + (g\sin(\alpha/\nu))f(x)^2(x_0)t. \tag{6}$$

Equation 2 thus has a solution

$$h = \left[\frac{1}{t}\frac{\nu(x-x_0)}{g\sin\alpha}\right]^{1/2} \tag{7}$$

At the limit $x_0 << x$ equation 7 becomes

$$h \to \left[\frac{1}{t}\frac{\nu x}{g\sin\alpha}\right]^{1/2}. \tag{8}$$

Equation 8, in conjunction with equation 4, produces a means of evaluating the length of the current

$$0 \le x \le x_N = \left(9A^{\frac{1}{2}}g\frac{\sin\alpha}{4\nu}\right)^{\frac{1}{3}} t^{\frac{1}{3}} \tag{9}$$

This may be written as a simple proportionality equation be combining the fluid dependent constant as $\hat{C_N} = \hat{t}/\hat{x_N}^{\frac{1}{3}}$

$$\hat{x_N} = \left(\frac{\hat{t}}{\hat{C_N}}\right)^{1/3} \tag{10}$$

At x_n the profile of the current ends with the height of $h_n(t) = 1.5A/x_n$. The solution may be smoothed by including higher order terms to account for the effects of surface tension.

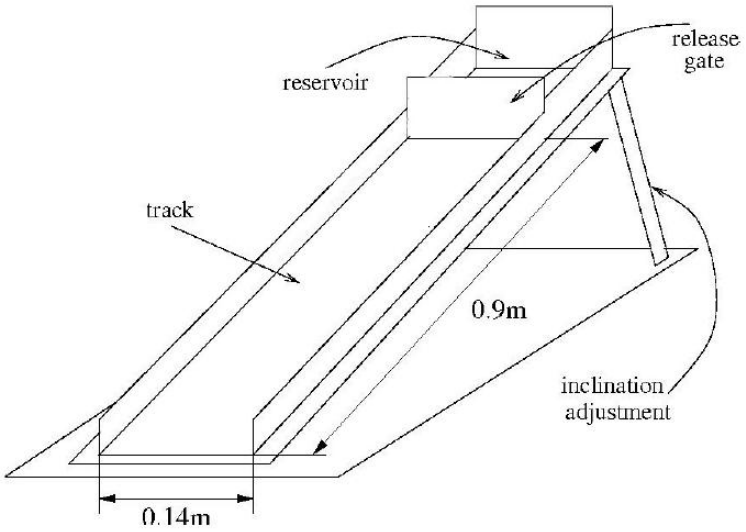

Figure 1: Experimental apparatus with adjustable incline

3 METHODS

3.1 EXPERIMENTAL SETUP

Figure 1 depicts the setup that is used to preform all the experiments. It consists of an acrylic track with adjustable inclination angle, α, which has a range of 5° - 80°. The track is 0.90m long and 0.14m wide, with 0.02m side walls. A liquid and particle mixture is produced in preparation for the run. This mixture is poured into the reservoir situated at the top of the track immediately before a run. The reservoir of dimensions height $\times$ width $\times$ length = 0.04m $\times$ 0.14m $\times$ 0.10m has a much larger volume than the prepared mixture. To begin the run the gate is lifted, allowing the mixture to flow down the track, with the contact line initially straight. Here, we only focus on experiments with finite, constant suspension volume. The evolution of the flow is monitored using a digital camera, which is positioned above the track and captures a video of the moving front. Using the setup shown in figure 2, we are able to monitor the film's motion, starting from 0.1 cm down the track, until the front has reached approximately 0.8 m down the track. This video is

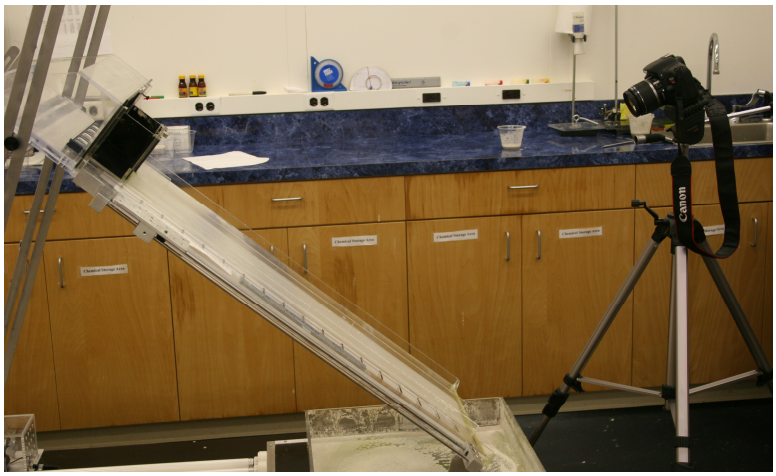

Figure 2: Pictured is the actual incline and positioned cammera

converted into still images by taking 1 frame from every 1 second interval of the video. Images and video are subsequently analyzed, and each experimental run is classified quantitatively by regime, the number of fingers, wavelength, the local particle concentration and if the two types of beads have separated. Our experiments involve two different particles, which are glass beads (GSB-5) and ceramic beads, mixed into silicon oil. The properties of the particles, which vary in density and diameter, are summarized in Table 1. The values represented are average densities and average sizes since the particles are polydisperse. In an attempt to purely examine the effect of a difference in the densities of the 2 types of particular the two types of beads were chosen to have smiler size and shape. Both types of particulate have a spherical shape and are of smiler size. The silicon oil used is polydimethylsiloxane (PDMS) with a kinematic viscosity of 1000cSt.

Suspensions are prepared by first weighing the particles and PDMS individually, pouring PDMS into a container, and then adding particles; slow manual stirring is used until uniform mixture is obtained. This is stired untill the mixture is emtyed into the reservoir. The two types of beads were dyed useing food coloring. After testing multiple colors on both ceramic and glass beads the two colors that provided the most contrast between the ceramic and GSB-5. This was done useing

Table 1: Particle Specifications

Particle	$\rho(g/cm^3)$	diameter (mm)
Ceramic	3.8	0.3 ± 0.1
GSB-5	2.475	0.39 ± 0.14

Matlab, of the average RGB values of picture of the beades was comapred. We wanted to get the 2 most distinct colors after dyeing.

3.2 IMAGE ANALYSIS AND PROCESSING

Automatic Ruler Line Detection

We use an custom algorithm utilizing image registration via normalized cross-correlation and image-subset selection to determine the location of ruler tick marks. These tick marks are then used to calculate a cubic fit to determine real-world distances while taking into account visual aberration due to the camera angle. The algorithm is written as a MATLAB function whose input is an RGB image and whose output includes cubic fit coefficients and conversions between pixels and centimeters. Selection of the image subset containing the ruler lines is done manually until either the program finds all the ruler lines correctly or the user opts to manually input their locations. The algorithm converts the RGB image to a grayscale one and creates a binary image of the edges via MATLAB's built-in Prewitt edge detection. The normalized cross-correlation of each pixel in the binary image is then calculated with respect to a customized binary straightedge. The highest matches are then assumed to be ruler lines.

Automatic Bi-Modal Thresholding

Another custom algorithm implemented automatic bi-modal thresholding to create a binary image of the slurry versus the background. Conscecutive RGB frames were subtracted, converted to

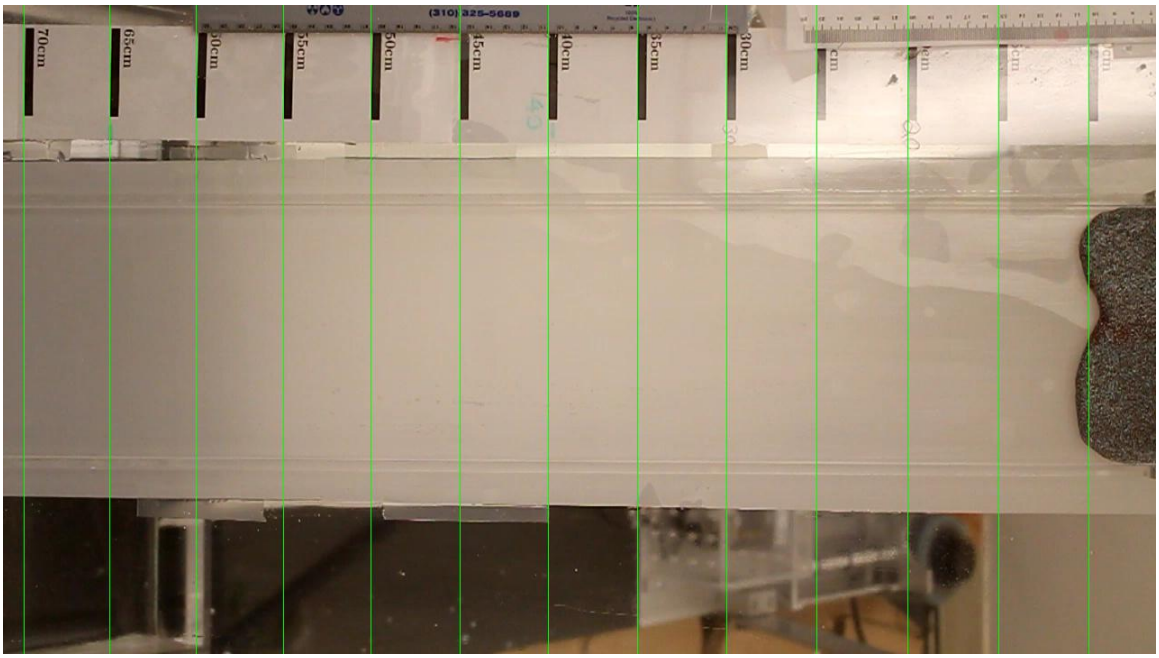

Figure 3: Example of the program finding all ruler lines automatically.

grayscale, and thresholded using Otsu's method. The resulting binary image was then filtered using MATLAB's default Wiener filter and a pre-set number of median filters to reduce noise and preserve the integrity of the slurry front. The algorithm then reads the locations of the slurry front and created plots of the instantaneous velocity and position of the slurry with respect to time. A linearized plot of the position versus time data was also generated to determine the time exponent of the fluids in the experiments for comparison with Huppert's model.

Issues with Settled Regimes

This was largely succesful in well-mixed and ridged regimes without large concentrations of GSB-5. Automatic bi-modal thresholding largely failed to accurately discern the slurry front for the settled regime because the front tracked was the clear oil. The edge of the oil was indicated by the reflection of light, which was problematic due to the inconsistency of the lighting. Thus, in settled cases, the front was tracked very poorly.

To track the front more accurately in settled regimes, we used MATLAB's built-in Canny edge

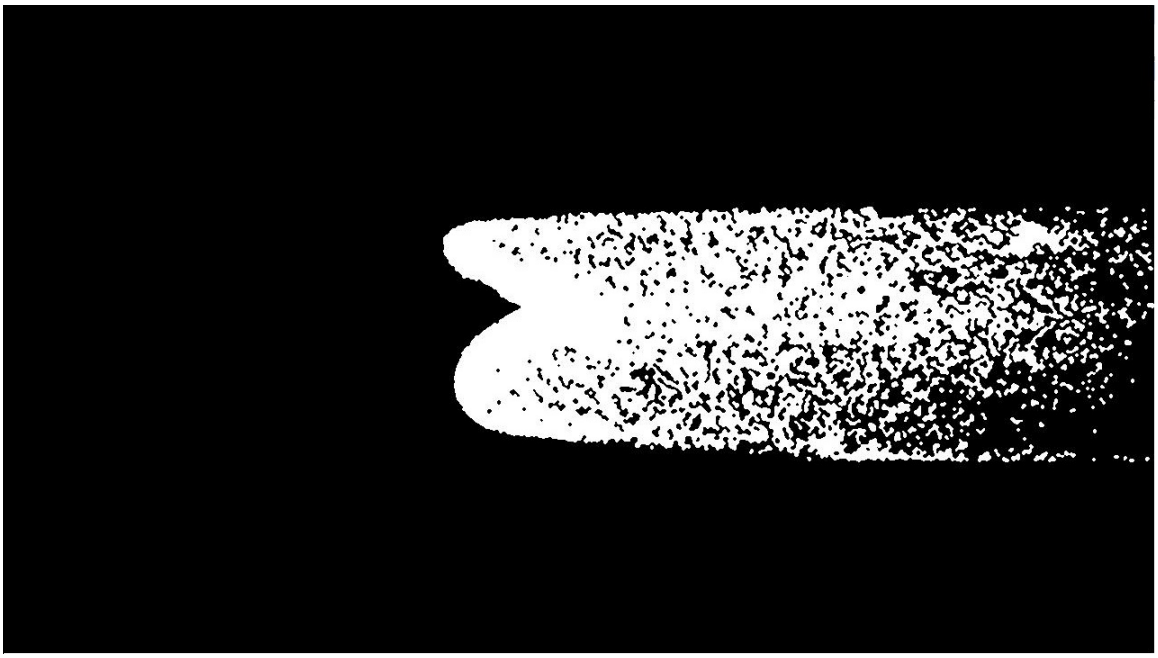

Figure 4: Example of the algorithm thresholding slurry and non-slurry.

detection algorithm with increased thresholds. While the slurry front was tracked more effectively in some settled cases, often no edge would be detected. Therefore, settled regimes pose a special problem to our image analysis algorithms.

Unanticipated problems encountered with image analysis also included the fluorescent lighting. The lights illuminating the slurry flicker at about 50 Hz. When the camera's shutter speed is not synchronized with the flickering of the lights, the difference between consecutive video frames shows these lighting differences. Thus, the binary images produced suffered from noise that impeded both thresholding and edge detection in the analysis of settled regimes.

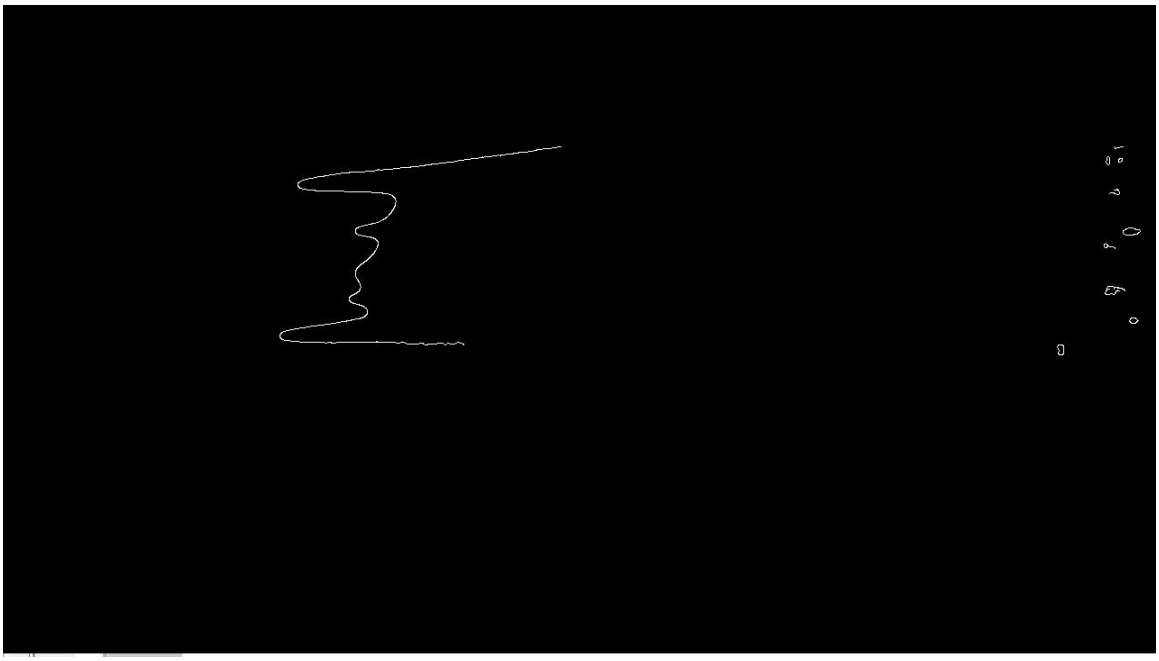

Figure 5: Example of the Canny edge detection algorithm's result with increased thresholds.

4 EXPERIMENTAL RESULTS

4.1 QUALITATIVE RESULTS

4.1.1 Flow Regimes

As the slurry mixture flowed down the track, we found that the particles within the slurry migrated in such ways that the overall flow would have different behavior depending on the initial conditions. We thus classified each run into one of three different qualitative regimes. The first regime we called 'settled', in this case, the particles settle on the substrate and separate from the fluid, which travels faster than the particles and allows for the formation of clear fingers. The second regime we call 'ridged;' in this regime, the particles travel to the front of the flow, creating a region of high particle density in the flow front. In the most extreme cases of this regime the particle concentration at the front reaches such high values, that portions of the flow break off and fall down the track. A third regime, which qualitatively falls in between the 'settled' and 'ridged' ones, was observed, in which the particles remain relatively homogeneously mixed with the fluid; we call this the 'well-mixed' regime. This 'well-mixed' regime is found to be a transient one: all runs start off in the well-mixed regime and then, depending on the initial conditions, the flow will go into either the ridged or the settled case. Figure 6 shows an example screenshot of each of the regimes.

We also classified each run into whether the glass and ceramic beads separated from each other: in some cases, the glass beads traveled faster than the ceramic ones, creating two clearly differentiable fronts. Figure 7 shows a separated and a mixed case.

Having classified each run into its respective flow regime and whether the particles separated or not (in the cases where only one bead species was present, the run was classified as 'separated'), we

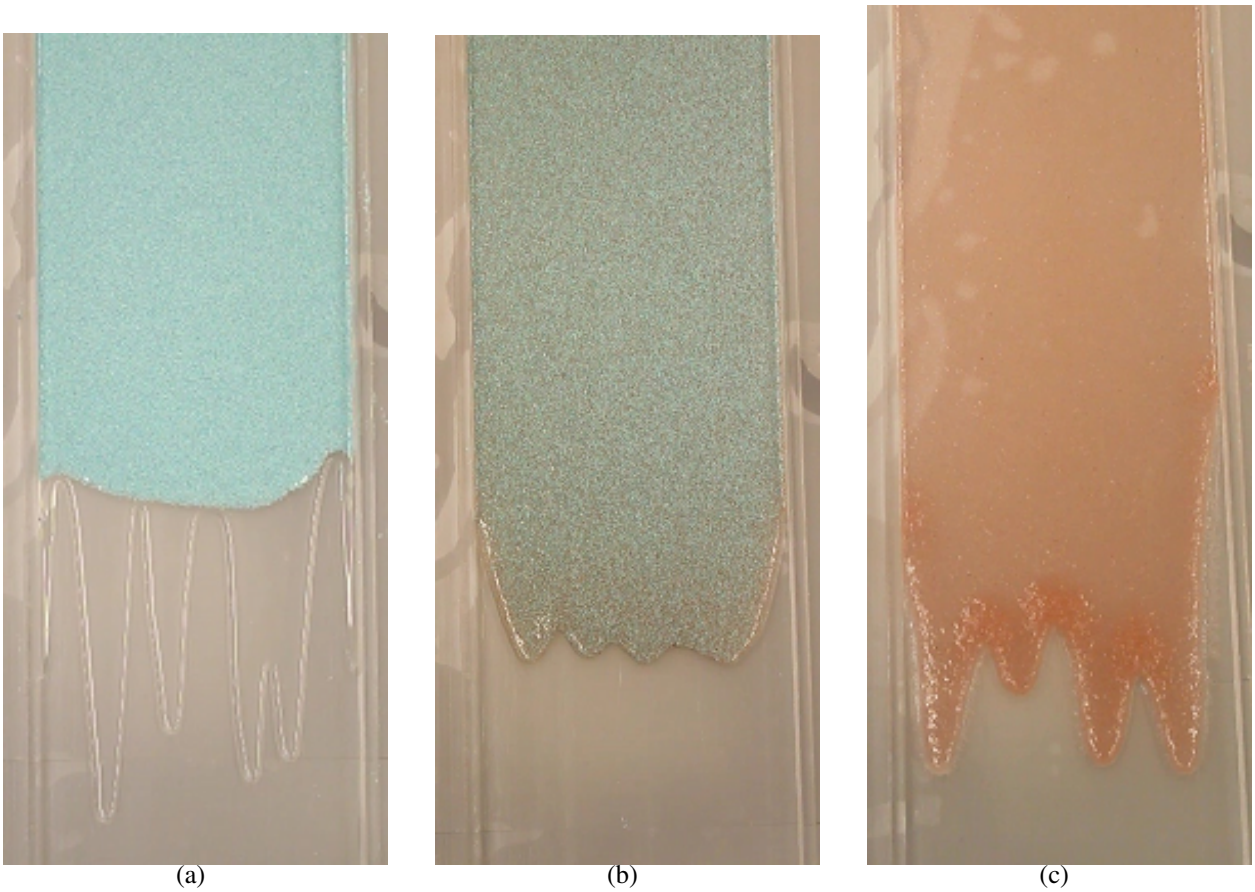

(a) (b) (c)

Figure 6: Screenshots of the three different possible regimes. All runs shown were done at an inclination angle of 30° and a total volume fraction of 0.4. (a) 0% GSB-5, settled regime, (b) 50% GSB-5, well-mixed, and (c) 100% GSB-5, ridged.

plotted the results according to their total volume fraction. Figure 8 shows the created plots

From Figure 8, we see that high angles and high GSB-5 beads ratio favor the ridged regime, whereas low angles and low GSB-5 ratio favor the settled regime. In the case of a 0.2 volume fraction (Figure 8 (a)), we see that for most angles the flow falls into the settled regime. With a 0.5 volume fraction (Figure 8 (c)), however, the flow mostly falls in the ridged regime. From this we see that low total volume fraction favors the settled regimes, whereas high total volume fraction favors the ridged regime, as is the case with mono-disperse flows [3]. However, the transient region

[3]Murisic et al., "Particle-laden viscous thin-film flows on an incline: Experiments compared with a theory based on shear-induced migration and particle settling." Physica D, 2011.

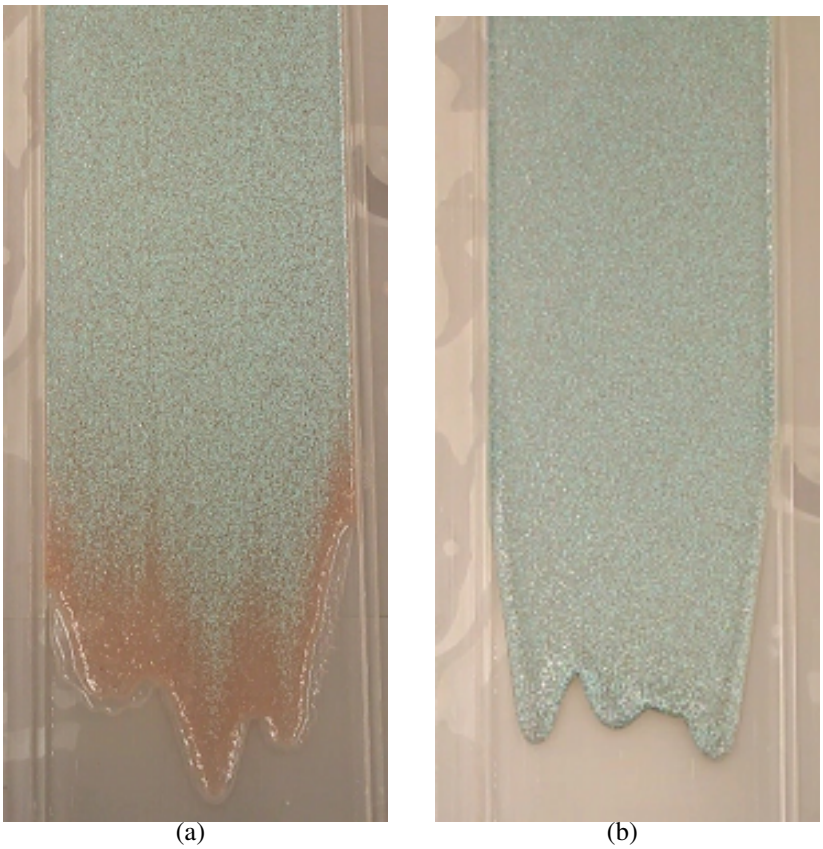

(a) (b)

Figure 7: Screenshots of the separated and mixed cases. Both runs were done with a volume fraction of 0.4 and a GSB-5:ceramic bead ratio of 50:50. (a) Inclination angle: $40°$, separated, (b) Inclination angle: $30°$, mixed.

(where we have the well-mixed regime) is found to be much smaller for the bi-disperse case than for the mono-disperse, suggesting that the flow when more than one beads species is present achieves its regime faster.

4.1.2 Particle distribution in the normal direction

An unexpected result was obtained when we noticed that the heavier ceramic beads seemed to be consistently on top of the lighter glass beads throughout the flow. This phenomenon was first seen when we dyed the GSB-5 red, and the ceramic beads blue. However, to rule out a possible optical illusion, we switched the color of each bead specied and did another run. The result was even clearer:

the ceramic beads migrted to the top of the flow, while the glass beads fell to the bottom. Figure 9 shows this phenomenon.

While the exact physics behind this result is unknown, this phenomenon is thought to be the result of competing forces in the direction normal to the flow arising from gravitational settling and shear-induced migration. In the direction of the flow, however, the lighter GSB-5 tend to travel faster than the heavier ceramic beads.

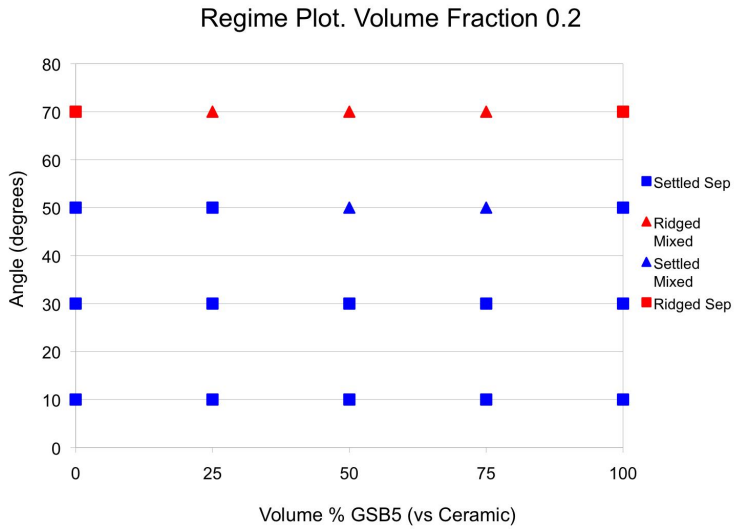

(a) $\phi = 0.2$

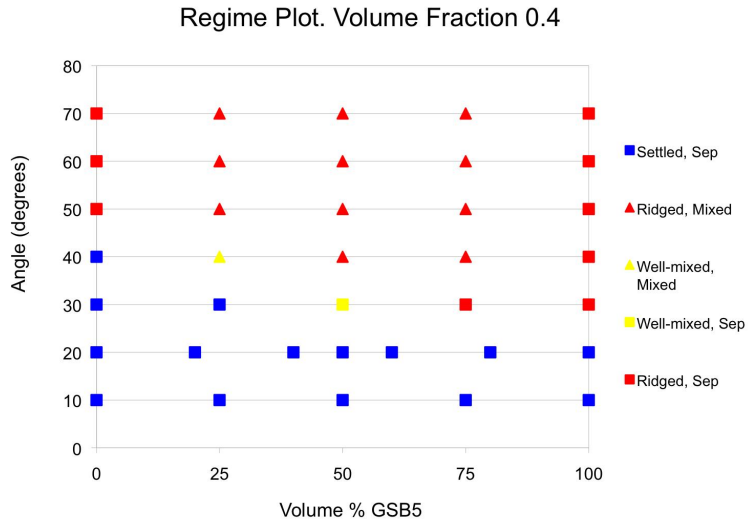

(b) $\phi = 0.4$

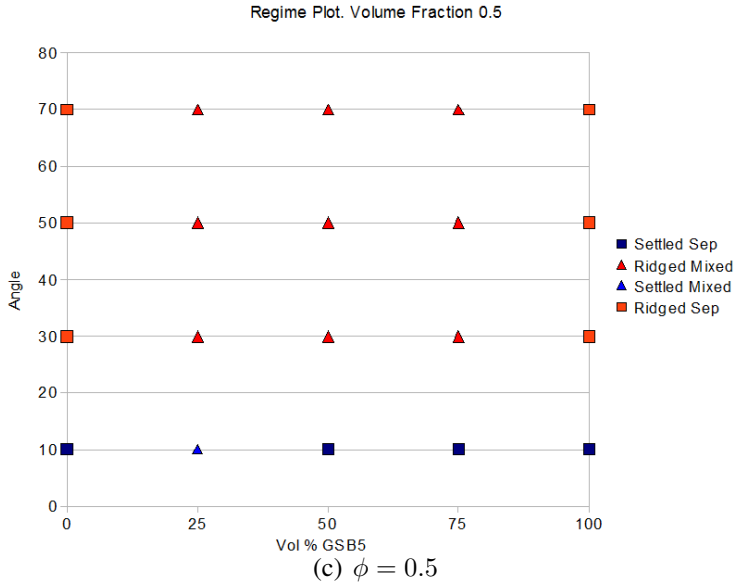

(c) $\phi = 0.5$

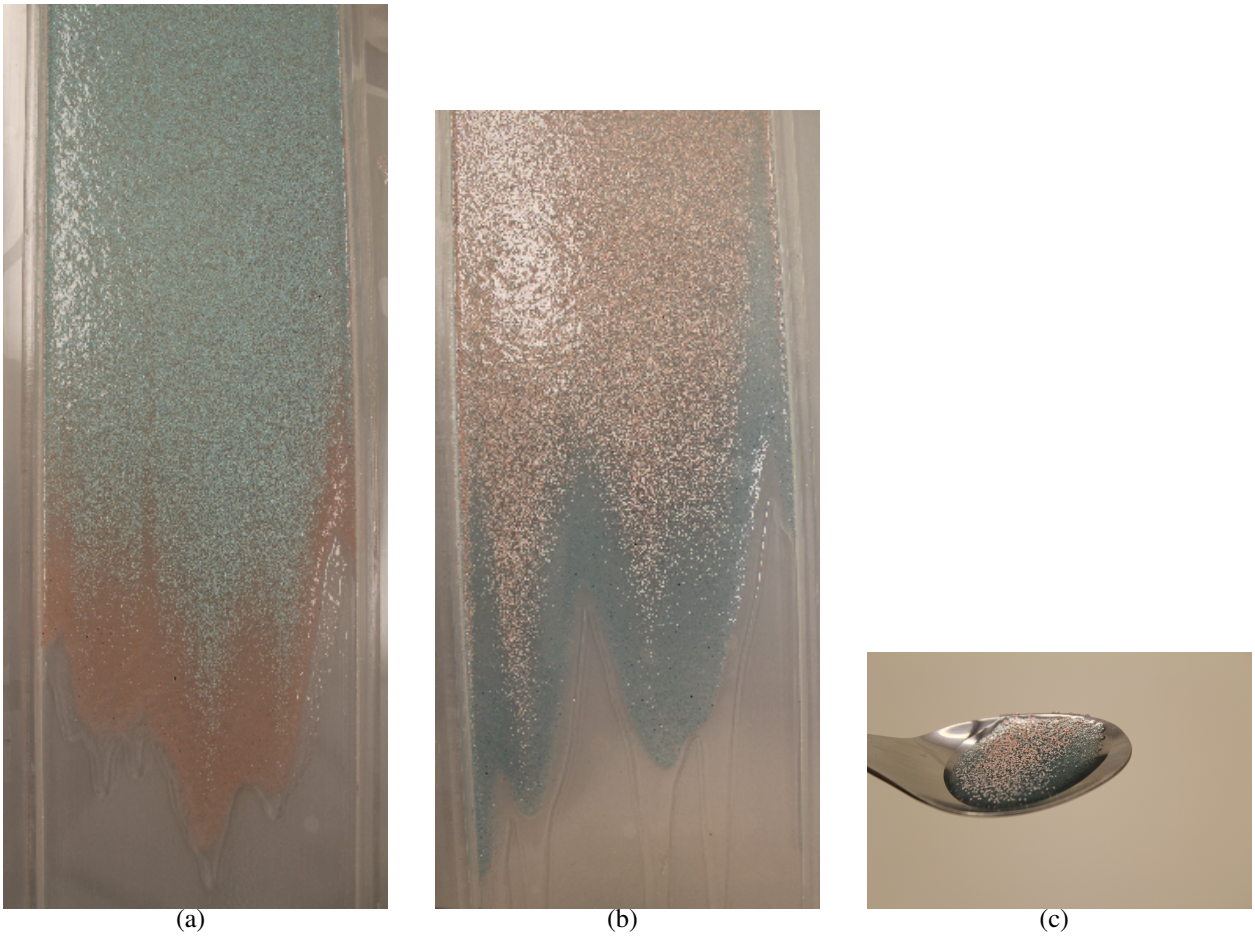

(a) (b) (c)

Figure 9: Photographs showing the heavier ceramic beads on top of the lighter GSB-5. (a) ceramic beads dyed blue, glass beads dyed red, (b) ceramic beads dyed red, glass beads dyed blue, (a) scoop on spoon of ceramic beads dyed red, glass beads dyed blue.

4.2 QUANTITATIVE RESULTS

4.2.1 Time Exponent and Velocity Results

We used MATLAB to output plots of the slurry front's average position versus time and log-position-log-time plots to compare the time exponent of the experiments with Huppert's model. We obtained average velocities as command window output. An example output from MATLAB for a run at 30 degrees, 0.5 volume fraction, and 75 percent GSB-5 relative to ceramic beads:

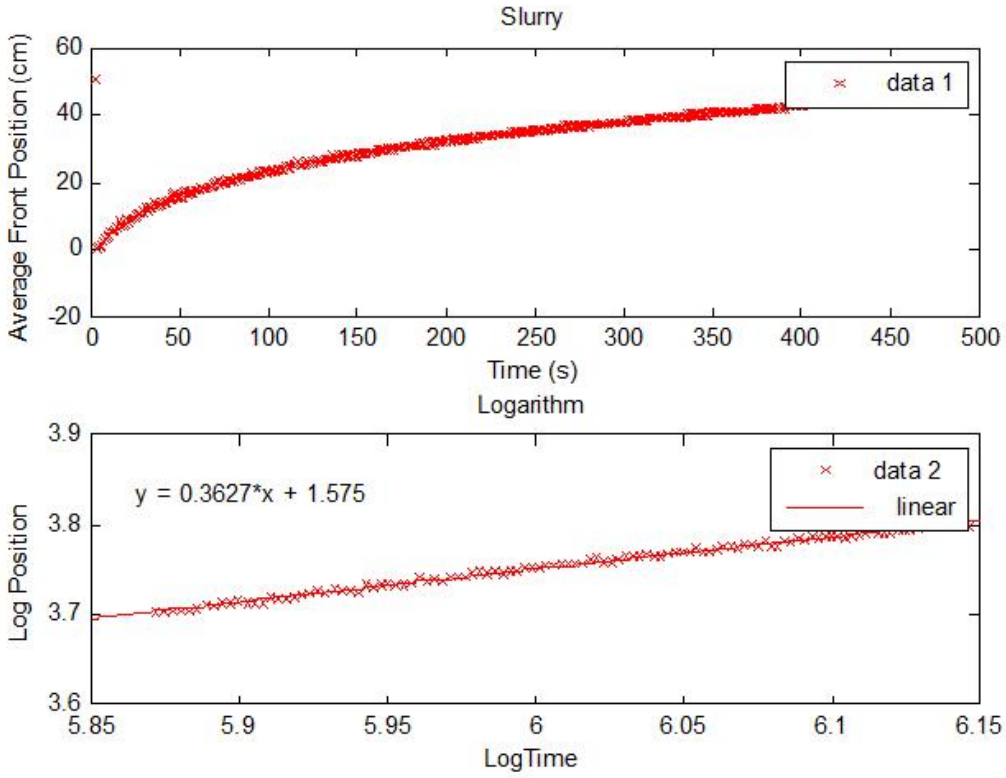

Figure 10: Example plot output from MATLAB.

In figure 10, it can be seen that the time exponent of this run was 0.3627 (a linear fit was used to determine this value). Note that only the last quarter of points were plotted when finding the linear fit because of the slowing of the slurry with time and a coding error which repeatedly produced an unusually high position for the first frame.

Using the exponent data collected from many of such graphs, we created a plot of the exponent values versus particle concentration to investigate the relationship between the concentration of each type of bead and the time exponent. Currently, we have completed such analysis for runs at 30 degrees, 0.4 volume fraction (settled and mixed regimes):

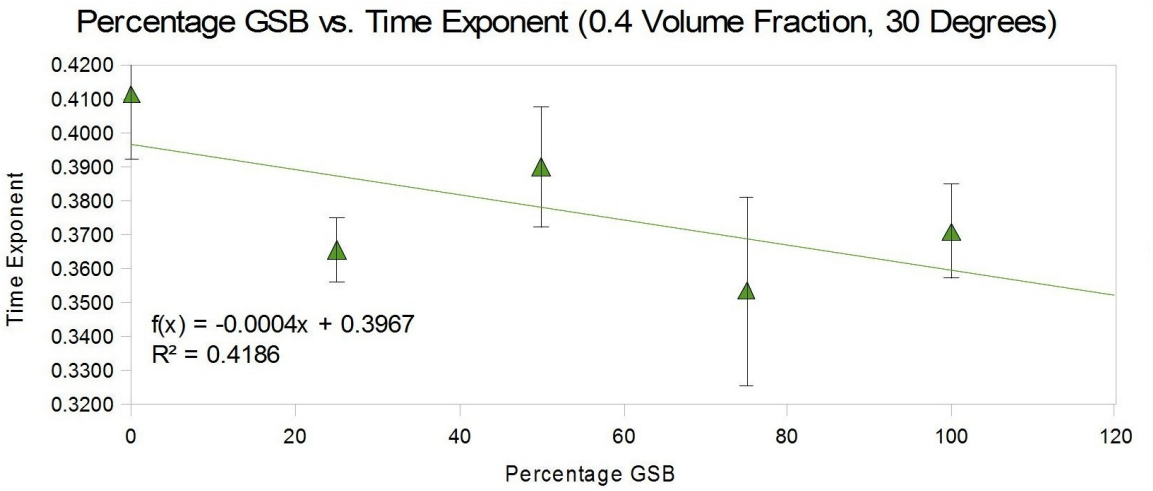

Figure 11: The miniscule slope indicates independence between percentage GSB-5 and the time exponent of the slurry.

The miniscule slope in figure 11 indicates that the time exponents (with the error bars showing one standard deviation) are not strongly affected by the percentage GSB-5 and is not significantly different from Huppert's value of $\frac{1}{3}$ for the time exponent. For settled regimes, we would expect the exponent to be $\frac{1}{3}$ because the front is clear fluid.

We also created plots of the average velocities (figure 12) versus the particle concentration to investigate the relationship between the concentration of each type of bead and the average velocity of the slurry front. Again, we have completed such analysis for runs at 30 degrees, 0.4 volume fraction (settled and mixed regimes):

As shown in figure 12, the slope is once again miniscule, indicating that the average velocities (with the error bars showing one standard deviation) are not strongly affected by the percentage

GSB-5. This may suggest that changing the bead concentrations did not significantly change the viscosity of the slurry.

4.2.2 Concentration Variations

In addition to tracking the average front position, we tracked the position of the GSB-5 and ceramic fronts separately using the red channel as a proxy for the GSB-5 beads and the blue as a proxy for the ceramic beads. To do this, we computed the average RGB values across the width of the slurry as a function of distance down the track. The resulting red and blue pixel profiles for three different times during the slurry flow are shown in figure 13. The position of each front approximately corresponds to the position of the sudden drop-off in pixel values (this is most clear for the red channel in figure 13), which has been identified by finding the x-coordinate with a pixel value equal to or greater than 87.5% of the maximum pixel value. This technique avoids the complication that the lighting is brightest halfway down the track, which prevents us from using the position of the maximum pixel value to track the position of the front. As the pixel values were averaged across the width of the slurry, heterogeneity in R and B values along the width of the slurry are not taken into account.

Using this technique, the location of the GSB-5 and ceramic fronts can be compared with each other. Plots of the front positions for two different runs are shown in figure 14. Both fronts follow the same general trend as the average front position did in figure 10, and in fact the time-dependence can be quantified using the same model.

The resulting time-dependence exponents for each run are shown in table 2. Note that these exponents cannot be directly compared with the average front position exponents, as the front position is calculated very differently in each case. Additionally, since Huppert's model holds for fluid

fingers and not ridged slurry flow, the exponent is not expected to be $1/3$. Though the exponents cannot be compared with average front position or with analytic and/or numerical results, they do give an estimation of how much the slurry is separating along its length: the run with 75% GSB-5 is visibly more separated than the run with 25% GSB-5, and this effect is mirrored in the difference between the ceramic and GSB-5 exponents for each run.

4.2.3 Average Wavelength

The average wavelength of a slurry is defined as the average distance between finger tips. We calculated this by determining the distance between the outermost two fingers and dividing by the total number of fingers minus one. This means that the maximum average wavelength is limited by the total track width, 13.97 cm. It is also affected by the total number of fingers, which ranged between 2 and 6 with a median of 3, though since the outermost finger tips do not always occur along the edges of the track, the total number of fingers does not fully determine the average wavelength. The average wavelength across all of the 0.4 volume fraction trials ranged from $2 - 8.5$ cm, with a mean of 3.99 cm and a median of 3.94 cm. The relationship between average wavelength and GSB-5 concentration is shown in figure 15. We do not yet have a theoretical prediction for the dependence of average wavlength upon GSB-5 concentration.

Time-Dependence Exponent

	25% GSB-5	50% GSB-5	75% GSB-5
GSB-5	0.42	0.391	0.404
ceramic	0.416	0.319	0.325

Table 2: Table of the exponent relatiing the front position to the time, as in Huppert's model.

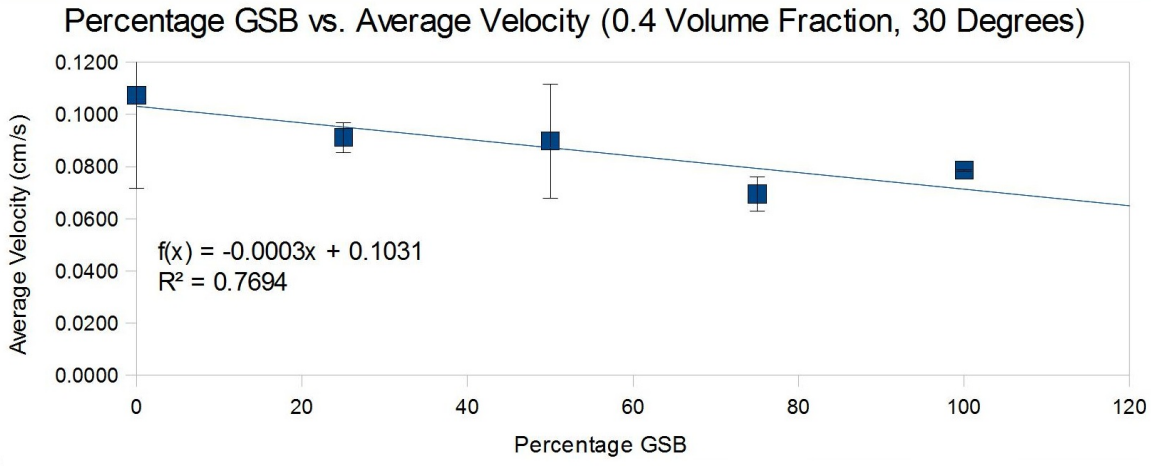

Figure 12: The miniscule slope indicates independence between percentage GSB-5 and the average velocity of the slurry.

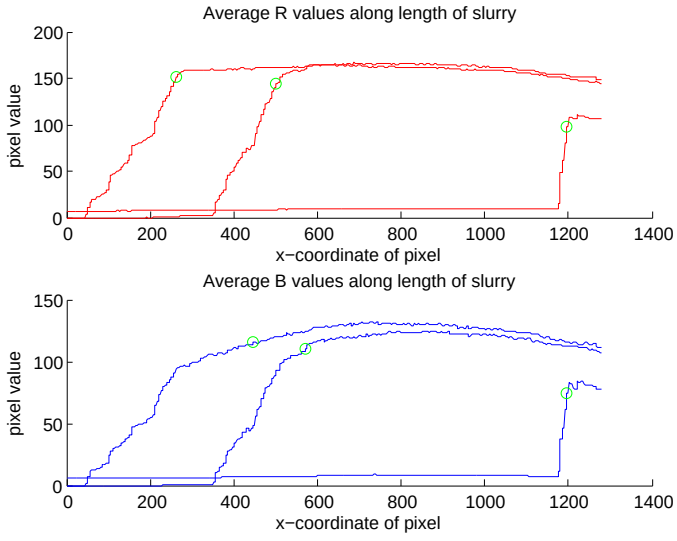

Figure 13: Average red and blue pixel values as a function of length along the track for three different images of the slurry flowing. Each profile corresponds to a different time in the flow of the slurry, with the earliest profile occuring the fartherst to the right. High x-coordinates correspond to the beginning of the track, and low to the end.

25% GSB-5

75% GSB-5

(a)

(b)

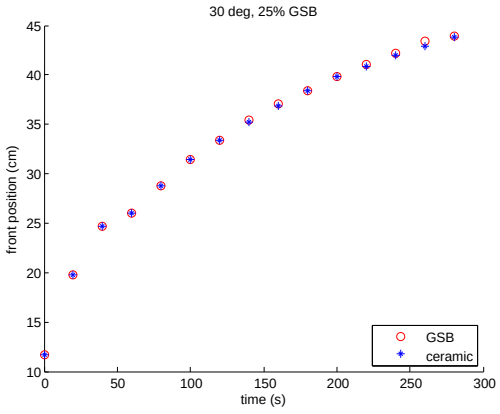

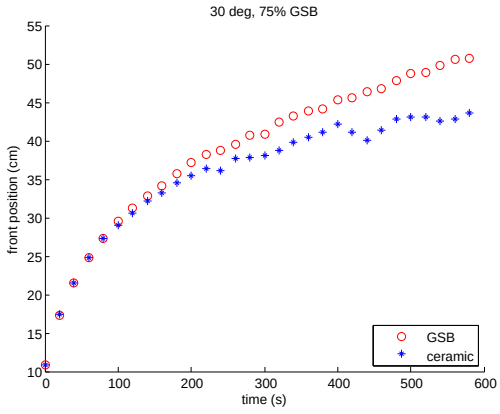

(c)

(d)

Figure 14: Plots of GSB-5 (red) and ceramic (blue) front positions as a function of time: (c) 25% GSB-5, which is well-mixed, and (d) 75% GSB-5, which is separated. Both runs were done at a 30 deg angle with 0.4 volume fraction.

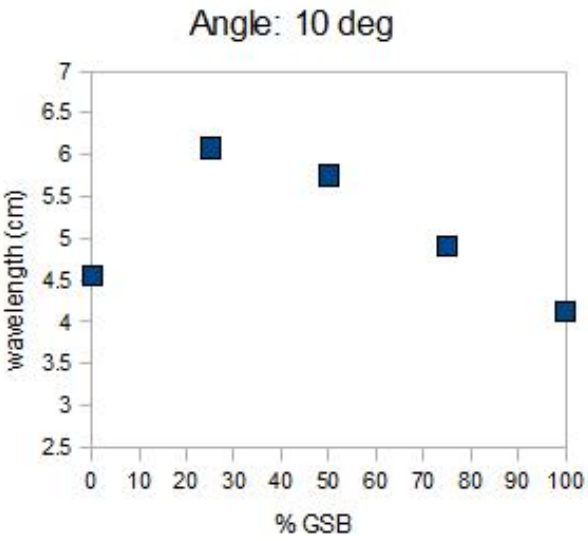
Angle: 10 deg
wavelength (cm)
% GSB

(a)

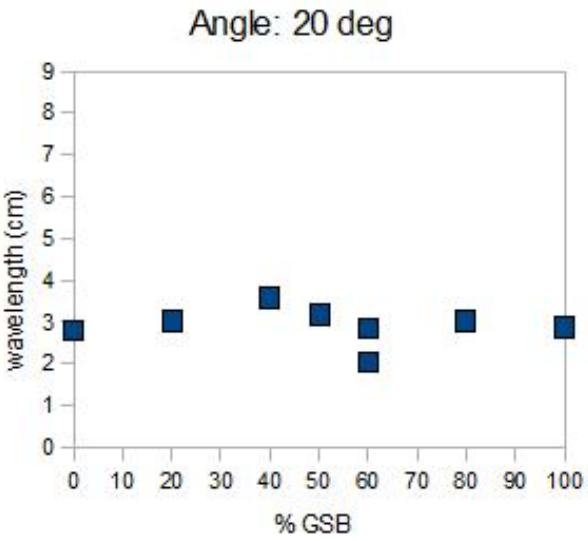
Angle: 20 deg
wavelength (cm)
% GSB

(b)

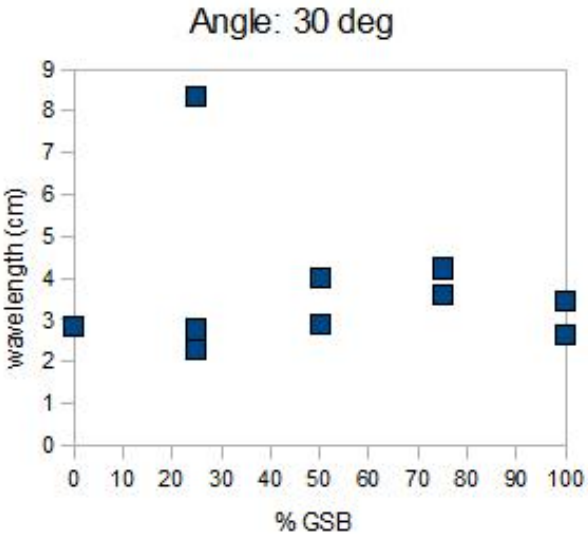
Angle: 30 deg
wavelength (cm)
% GSB

(c)

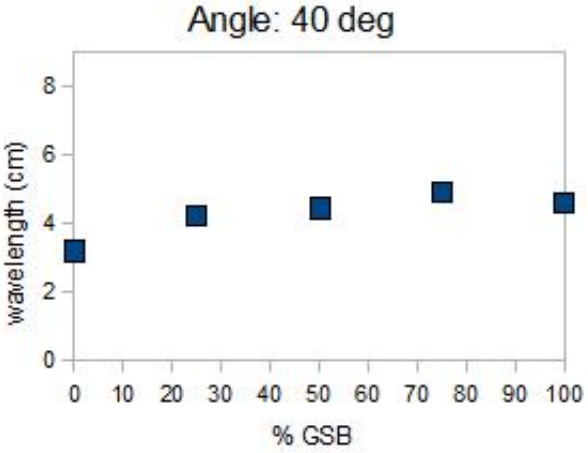
Angle: 40 deg
wavelength (cm)
% GSB

(d)

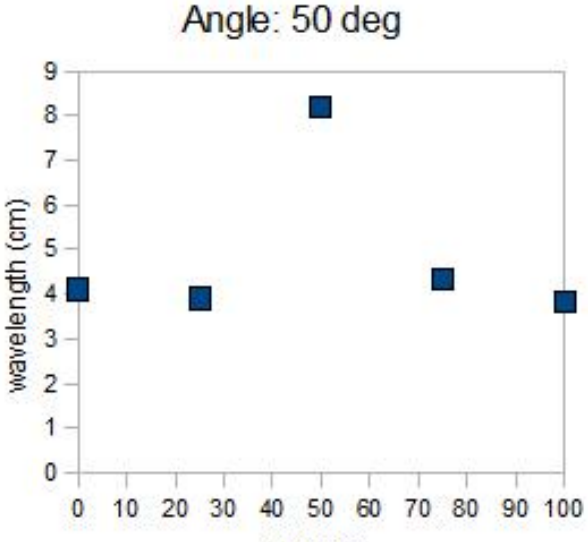
Angle: 50 deg
wavelength (cm)
% GSB

(e)

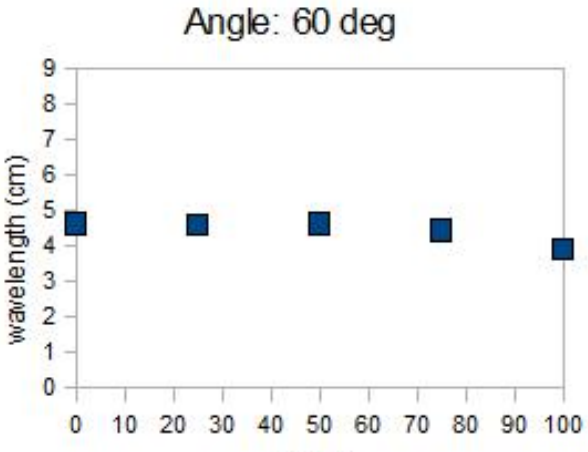
Angle: 60 deg
wavelength (cm)
% GSB

(f)

5 FINAL MODELING

We study a dense suspension flow on an incline, consisting of negatively buoyant particles with uniform size in a viscous suspending liquid. For modeling purposes we concentrate on the settled regime, where gravity drives the flow down an incline and leads to stratification of the suspension. The model is based on Stoke's equations for an incompressible variable-viscosity suspension and the conservation of total mass of particles. We consider the continuum limit, including the effects of hindered settling and shear-induced migration. Due to the difference in the relevant timescales, a fast one for the settling and a slow one for the suspension flow, we assume that the particle distribution is in equilibrium along the direction normal to the solid substrate while the particles are transported along the solid substrate.

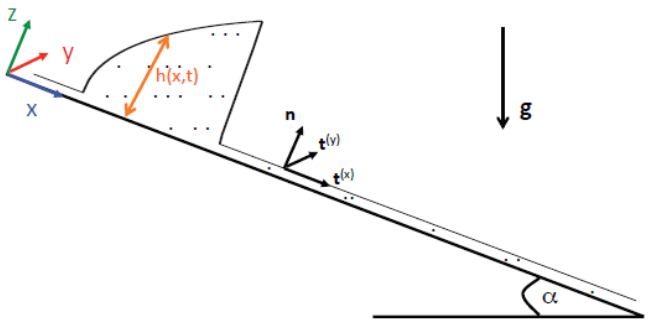

Figure 16: Schematic of inclined plane with particle slurry

Figure 16 shows the set up. The z and x-coordinates are in the directions normal to and along the solid substrate respectively. The solid substrate is located at z = 0 and the free surface of the suspension at z = h(x,t). The angle of inclination of the solid is α. We focus on the settled regime for which a dense sedimentation layer of particles forms close to the substrate with a clear fluid layer on top of it. At each time, t, and point (x,z) the particle volume fraction, $0 <= \phi(t, x, z) < 1$, and

the volume averaged velocity, **u**(t,x,z) = (u(t,x,z), w(t,x,z)), are defined. The upper bound for ϕ constitutes the maximum random packing volume fraction. This was estimated experimentally [4] as $\phi_m = 0.61$.

5.1 TWO-PHASE MODEL AND LUBRICATION EQUATIONS

We begin with the following system of PDEs for the particle volume fraction $\phi \in [0, \phi_m]$ and the suspension velocity **u**.

$$\nabla \cdot \mathbf{\Pi} = f \tag{11}$$

$$\phi_t + \mathbf{u} \cdot \nabla\phi + \nabla \cdot \mathbf{J} = 0 \tag{12}$$

The first equation 11 represents a balance of linear momentum for the suspension, where Π is the stress tensor and the buoyancy is taken into account via $\mathbf{f} = (\rho_p\phi + \rho_l(1-\phi))$ **g** with the acceleration of gravity given by **g** =$g(\sin(\alpha), -\cos(\alpha))$. The dependence of the suspension viscosity on ϕ is included through the Krieger-Dougherty relation $\mu = \mu_l(1 - \frac{\phi}{\phi_m})^{-2}$ [5] and [6]. The second equation 12 represents the conservation of particle mass, where the particle fluxes are defined as in Murisic et al.

$$\mathbf{J} = \mathbf{J}_{grav} + \mathbf{J}_{coll} + \mathbf{J}_{visc} \tag{13}$$

where,

[4] Murisic et al, 2011, Physica D: Nonlinear Phenomena 240, 1661
[5] Van Der Werff and De Kruif (1989) J. Rheol. 33
[6] Brady (1993) J. Chem. Phys. 99, 567.

$$\begin{aligned} \mathbf{J}_{grav} &= \frac{d^2\phi(\rho_p - \rho_l)}{18\mu_l} f(\phi)\mathbf{g} \\ \mathbf{J}_{coll} &= -\frac{K_c d^2}{4}\left(\phi\nabla\dot{\gamma} + \phi\dot{\gamma}\nabla\phi\right) \\ \mathbf{J}_{visc} &= -\frac{K_v d^2}{4\mu}\phi^2\dot{\gamma}\mu_\phi\nabla\phi. \end{aligned} \tag{14}$$

The terms in the first brackets take into account the effects of shear-induced migration while the terms in the second bracket represent the hindered settling of particles due to gravity. K_c and K_v are empirical constants for which we use K_c = 0.41 and K_v = 0.62 [7]. The particle diameter is d and the shear rate is given by $\dot{\gamma} = \frac{1}{4}\|\nabla\mathbf{u} + \nabla\mathbf{u}^T\|$

Equations 11 and 12 are accompanied by the incompressibility condition:

$$\nabla \cdot \mathbf{u} = 0 \tag{15}$$

and the following boundary conditions: no-slip and impermeability at the solid substrate, u = w = 0 at z = 0; the zero shear stress condition at the free surface, $\mathbf{t} \cdot \mathbf{\Pi n} = 0$ at z = h; and the zero particle flux conditions at both interfaces, $\mathbf{J} \cdot \mathbf{n} = 0$ at z = 0 and z = h; where n is the outward pointing normal vector and t is the tangential unit vector at the free surface. The free surface evolves according to the kinematic condition $\partial_t h = w - u\partial_x h$ at z = h.

Equations 11 and 12 are then scaled using the lubrication approximation. [8] In order for the equilibrium assumption to hold we require that the typical distance a particle travel in the x-direction is asymptotically smaller than the lubrication length scale $[x] = \frac{H}{\epsilon}$ where H is the typical scaling in

[7] Phillips et al. (1992) Phys. Fluids A 4, 30

[8] Kondic and Bertozzi, 1999 Phys. Fluids 11, 3560l.

the normal direction and ϵ is the small lubrication parameter. Hence we need to consider:

$$\epsilon << \eta^2 << 1 \tag{16}$$

where $\eta = \frac{d}{H}$. We can achieve this by setting $\epsilon^\beta = \eta^2$. Applying the scales to conservation of total mass of particles gives:

$$\begin{aligned} \phi_t + u\phi_x + w\phi_z &= \frac{-\epsilon^\beta \rho_s}{18}\left[(\phi f(\phi))_x - \epsilon^{-1}\cot\alpha\,(\phi f(\phi))_z \right] \\ &+ \frac{\epsilon^\beta K_c}{4}\left[\epsilon\left(\phi^2\dot{\gamma}_x + \phi\dot{\gamma}\phi_x\right)_x + \epsilon^{-1}\left(\phi^2\dot{\gamma}_z + \phi\dot{\gamma}\phi_z\right)_z \right] \\ &+ \frac{\epsilon^\beta K_v}{4}\left[\epsilon\left(\frac{\phi^2}{\mu}\gamma\frac{d\mu}{d\phi}\phi_x\right)_x + \epsilon^{-1}\left(\frac{\phi^2}{\mu}\gamma\frac{d\mu}{d\phi}\phi_z\right)_z \right], \end{aligned} \tag{17}$$

keeping leading order terms, i.e. $\mathcal{O}(\epsilon^{\beta-1})$ we obtain:

$$\sigma\phi'\left[1 + \frac{2\phi}{(\phi-\phi_m)}\left(\frac{K_v - K_c}{K_c}\right)\right] + \phi\sigma' + \frac{2\rho_s\cot\alpha}{9K_c}(1-\phi) = 0. \tag{18}$$

Similarly, from the Stokes equations we obtain the following ODE for the shear stress, σ

$$\sigma' = -(1 + \rho_s\phi) \tag{19}$$

where prime denotes differentiation with respect to z.

We now have two explicit ODEs for the total volume fraction (18) ϕ and the shear stress σ (19) which can be solved in Matlab.

5.2 BI-DISPERSE MODEL

In order to produce numerical simulations for the bi-disperse flow we concentrate on the settled regime. We assume a layered model with separation in the z-direction: At the boundaries between

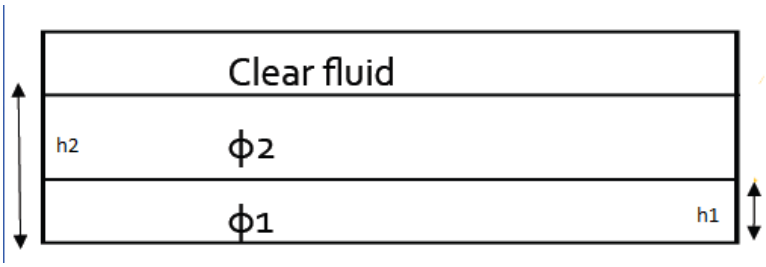

Figure 17: Layered model

each of the layers we match both the velocity and the shear stress.

There are two cases we will consider: lighter particles on top as expected intuitively and heavier particles on top as observed in the experiments.

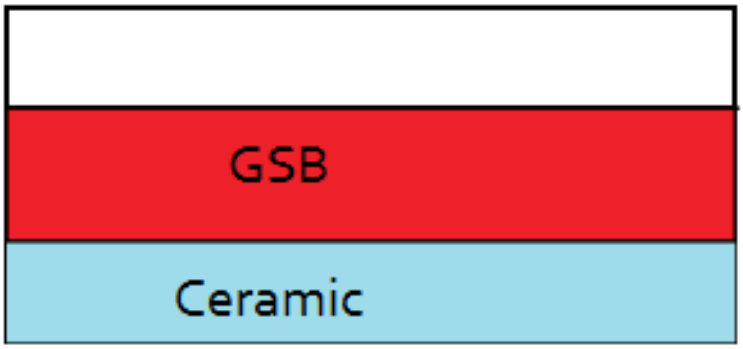

Figure 18: Heavier ceramic beads settle to the bottom of the flow

The system of ODEs (18) and (19) are solved in Matlab for each height h_1 and height h_2, where h_1 varies linearly between ϵ (10^{-12}) and 0.9 and h_2 varies linearly between $h_1 + \epsilon$ and $1 - \epsilon$, both in 50 steps. The individual volume fractions (ϕ_1, ϕ_2), velocity, and various fluxes of interest. We concentrate on the velocity profiles to see whether the numerical simulations will produce the same phenomena seen in our experiments, i.e. can we have the heavier ceramic beads on top with the

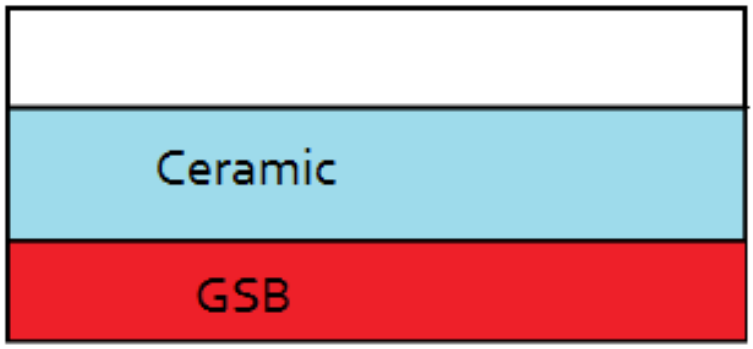

Figure 19: Heavier ceramic beads on the top of the flow - as seen in the experiments

lighter GSB-5s moving faster?

Below are the velocity profiles obtained for simulations with a volume fraction of 0.2, an angle of 30 degrees, and ceramic to GSB-5 particle ratios of 25:75, 50:50 and 75:25 respectively. The first set of figures is with the heavier ceramic beads on top of the lighter GSB-5s and the second set is with the GSB-5s on top of the ceramic beads.

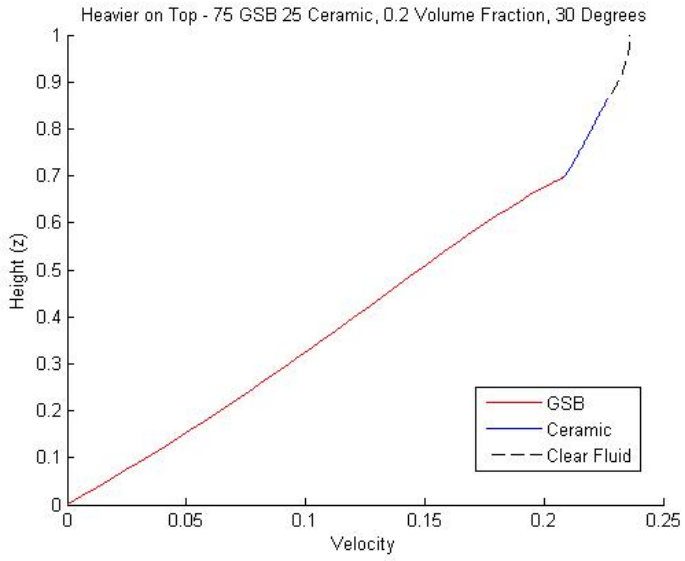

Figure 20: Velocity profile for heavier beads on top, with a particle ratio of 25:75, ceramic to GSB-5

With the ceramic beads at the top of the flow, the velocity profiles show the ceramic beads to be moving at a higher velocity than the GSB-5s beneath them. This is contradictory to our experimental

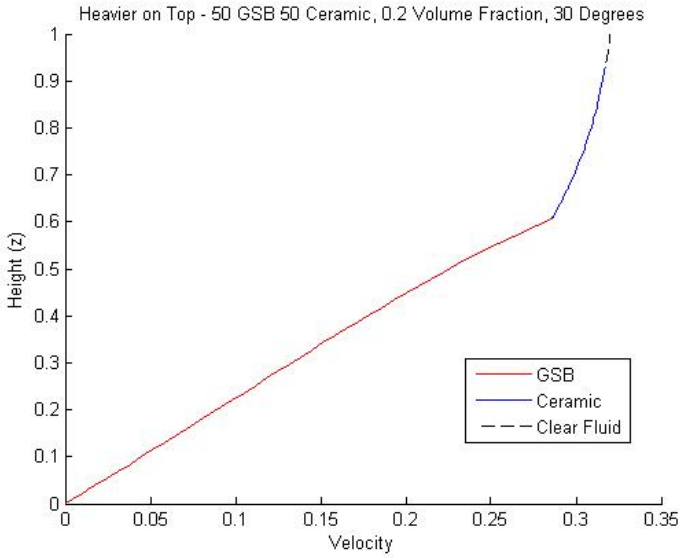

Figure 21: Velocity profile for heavier beads on top, with a particle ratio of 50:50, ceramic to GSB-5

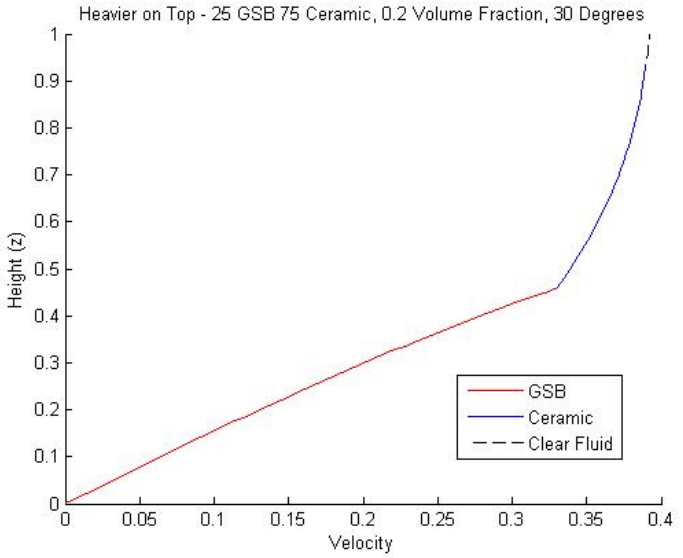

Figure 22: Velocity profile for heavier beads on top, with a particle ratio of 75:25, ceramic to GSB-5

results, where the GSB-5s would always be seen to be moving faster than the ceramic beads. In contrast, with the GSB-5 beads on top of the ceramic beads, the velocity profiles show that the GSB-5s do indeed have a greater velocity than the ceramic beads, agreeing with the trend seen in the experiments. In this instance, however, the order of the layering of the beads does not match

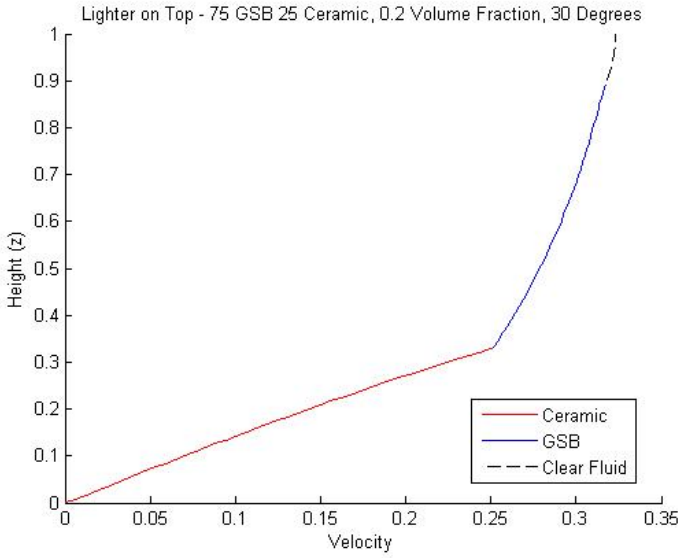

Figure 23: Velocity profile for lighter beads on top, with a particle ratio of 25:75, ceramic to GSB-5

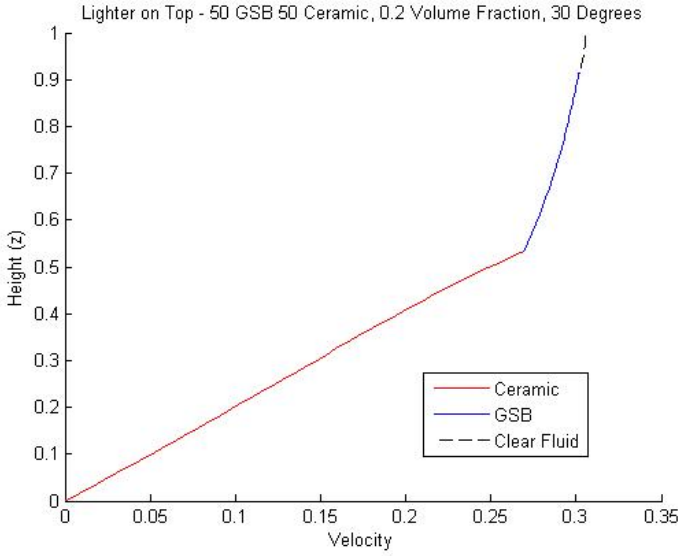

Figure 24: Velocity profile for lighter beads on top, with a particle ratio of 50:50, ceramic to GSB-5

that seen experimentally and therefore neither set of results demonstrate the phenomena seen in the experiments.

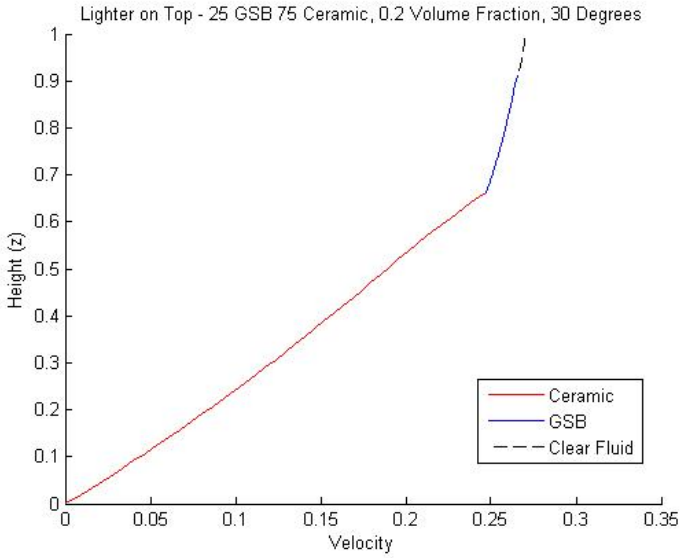

Figure 25: Velocity profile for lighter beads on top, with a particle ratio of 75:25, ceramic to GSB-5

6 CONCLUSION AND FUTURE WORK

Among our most relevant experimental results, we found that the lighter GSB-5, if they separate from the ceramic beads, tend to travel faster down the incline than the ceramic beads. We also found that the ceramic beads, while heavier, migrated above the lighter glass beads. While this phenomenon is not entirely understood, we found enough evidence to hold it as true. Another property we found about the ceramic beads was that they induce settling of the flow, that is, while a flow of glass beads would normally go into the ridged regime, as we increase the proportion of ceramic beads we go through the well-mixed, and into the settled regime.

While the current model takes into account the presence of three different layers, it takes them as three pure layers, each with either fluid, or ceramic or glass beads. In reality, however, the beads are mixed throughout the flow, especially towards the beginning of each run, where all flows start off as well-mixed. Thus, an improvement of this model is sought in the future. During this project, we also experimented using beads of different sizes. Once the physics of the experiments presented are better understood, we plan to move on and introduce yet another variable: bead size.